PAPER

Check for updates

Mechanistic study of a CO-free pathway in the methanol oxidation reaction over oxygen vacancies in NiOOH

Thy Ho, Quy P. Nguyen [ID] and Bin Wang [ID] *

The methanol oxidation reaction is a key reaction in direct methanol fuel cells. Prior research indicates that if oxygen vacancies in NiOOH serve as the active sites, the methanol oxidation mainly proceeds through the formate-involving pathway, which is a CO-free pathway, distinct from the conventional path over transition metal catalysts, though the fundamental reason for this suppressed CO formation is unclear. Herein, we report density functional theory calculations, through which we uncover the underlying reasons for this alternate path of methanol oxidation over the oxygen vacancies in NiOOH. We find that the existence of oxygen vacancies in NiOOH affects the adsorption configuration of adsorbates and that the interfacial charge transfer is minimal for CHO and CO intermediates. In addition, CHO, a key intermediate to form CO, adsorbs at the oxygen vacancy through the oxygen atom, leading to low stability due to the incomplete valence saturation of the carbon atom. This weak electronic interaction and instability effectively inhibit CHO formation and, consequently, CO formation. These insights provide valuable guidance for the development of efficient and CO-tolerant catalysts for methanol oxidation.

Introduction

The methanol oxidation reaction (MOR) is critical in direct methanol fuel cells (DMFCs), which directly convert chemical energy from methanol into electrical energy, offering a sustainable energy source.[1–7] This MOR is of great interest due to its potential applications in portable electronics and automotive industries, driven by the need for sustainable, compact, and environmentally friendly power solutions.

Recent advances in catalysis have improved the MOR activity; however, efforts to address the destructive activity loss caused by unavoidable CO generation and surface passivation over transition metal catalysts during the MOR have been a challenge.[8,9] Among the non-noble catalysts, nickel has garnered significant attention due to its good catalytic activity, high tolerance to CO poisoning, cost-effectiveness, and earth abundance, making it a promising candidate for the MOR under alkaline conditions.[10–12] A variety of Ni-based catalysts for the MOR have been developed, such as $Ni(OH)_2$,[13] Ni alloys,[14–16] carbon-supported Ni catalysts,[17–19] Ni-based core–shell structures,[20,21] spinel structures,[22] and NiO nanosheets,[23] all exhibiting improved catalytic performance, stability, and resistance to CO poisoning. Notably, the onset potential for the MOR on monometallic Ni catalysts remains excessively high, hindering their effectiveness in DMFCs.[24] A detailed understanding of the

MOR mechanism and the nature of the active sites over Ni-based catalyst surfaces is thus valuable.

It has been shown that undercoordinated Ni can improve electronic conductivity and methanol adsorption, enhancing the overall electrocatalytic MOR performance,[13,23] and the oxidation of the alcohol is often accompanied by a change in the valence of the Ni cations (Ni^{2+}, Ni^{3+}, and Ni^{4+}).[25] Oxygen vacancy formation has also been considered valuable for electro-oxidation of alcohols.[26,27] For example, it has been shown that a vacancy-driven oxidation of benzyl alcohol over a Ni–Fe catalyst has a lower overpotential than the redox reaction mechanism.[28] We recently demonstrated that oxygen vacancies could form on the NiOOH surface concurrently at the onset potential of the MOR and that these vacancies could serve as active sites.[29] We showed that the MOR towards formate and (bi)carbonates could proceed through multiple routes and that none of the routes involved are thermodynamically favourable. Our previous work necessitates a deeper understanding of the mechanism underlying this behaviour of the MOR over the oxygen vacancies of NiOOH. Particularly, it is valuable to explore the fundamental reason that oxygen vacancies prohibit the CO formation.

Herein, we have employed density functional theory (DFT) calculations to understand how the interaction between the adsorbates and the O-vacant active site affects the thermodynamic stability of specific surface species, especially in those leading to CO formation. We have found that the stability of the CHO adsorbate on the surface influences the transition from CH_3O to CHO, which involves dehydrogenation through OH^-

School of Sustainable Chemical, Biological and Materials Engineering, University of Oklahoma, Norman, OK 73019, USA. E-mail: wang_cbme@ou.edu

insertion and water removal. We have observed very limited charge transfer between the oxygen in CHO and the oxygen vacancy in the NiOOH surface. We show that the particularly high energy of CHO could be attributed to the insufficient valence of the carbon, which significantly decreases the thermodynamic stability of CHO and thereby obstructs the formation of CO that demands crossing the CHO intermediate. This insufficient valence of the carbon in CHO is further determined by its adsorption configuration at the oxygen vacancy of NiOOH, which is distinct from the conventional transition metal catalysts like Pt. This work thus provides guidelines for designing more effective and robust catalysts for CO-free MOR processes.

Computational methods

Spin-polarized DFT+U calculations were carried out using the Vienna *ab initio* Simulation Package (VASP),[30] as we reported previously.[29,31] The PBE+U method[32] was applied with the effective interaction parameter (Hubbard U-value) set to 6.6 eV for Ni, as described in the literature.[33] The electron–ion interactions were described by the projector augmented wave (PAW) method, and a plane-wave cut-off energy of 400 eV was set.[34] The Perdew–Burke–Ernzerhof (PBE) exchange–correlation functional within the generalized gradient approximation (GGA) was employed.[35] The DFT-D3 semi-empirical approach was used to account for the van der Waals interactions.[36] A $1 \times 1 \times 1$ k-point mesh centred at the Gamma (Γ) point was used to perform the Brillouin zone sampling. A β-NiOOH (0001) supercell (4×4) was constructed using the unit cell described in the literature.[37] The corresponding groups (oxygen or OH) were eliminated from the surface to generate the oxygen vacancies.[29] To compare the transferred charges between the surface and different adsorbates, a Bader charge analysis was conducted.[38,39] Charge density difference was calculated as follows:

$$\Delta\rho = \rho_{total} - \rho_{O\text{-}vacantNiOOH} - \rho_{molecule}$$

where ρ_{total}, $\rho_{O\text{-}vacantNiOOH}$, and $\rho_{molecule}$ represent the charge density of the adsorbate on the O-vacant NiOOH surface, the O-vacant NiOOH surface, and the adsorbate, respectively; the latter two structures were kept at their optimized structures.

Results and discussion

Fig. 1 shows several possible reaction paths of the MOR in basic solutions. Methanol is first oxidized through two dehydrogenation steps (two one-electron steps) to form an adsorbed formaldehyde (CH_2O^*), which can then proceed along two parallel pathways to form $CH_2(OH)O^*$ and CHO^*, respectively, through OH insertion and dehydrogenation. The subsequent dehydrogenation process can produce CO^* from CHO^* or $CH(OH)O^*$ from $CH_2(OH)O^*$, respectively. The adsorbed CO^* can either desorb from the catalyst surface or undergo further oxidation to form $C(OH)O^*$, which then deprotonates to produce CO_2. In parallel, $HCOO^*$ can be generated from the deprotonation of $CH(OH)O^*$ by solvated OH^-, and then the $HCOO^*$ can be further oxidized to CO_2 and carbonate.
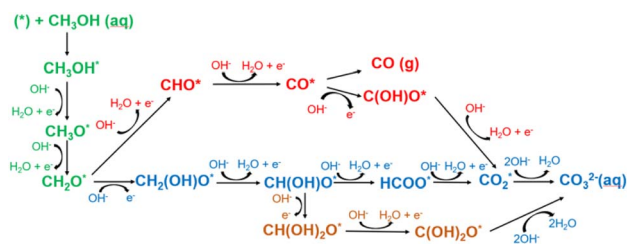

Fig. 1 Illustration of the competing reaction paths of the MOR in basic solutions. The green species are shared intermediates along the different reaction paths, and the distinct intermediates are highlighted in red (CO-involving path), blue (CO-free path), and brown (formic-free path), respectively.

We previously reported the energy profile of MOR on the O-vacant NiOOH, showing that conversion of CH_2O^* to CHO^*; the latter is a precursor to form CO^*, which is thermodynamically impeded over the competing route to form $HCOO^*$ through $CH_2(OH)O^*$.[29] In addition to this suppressed CHO formation (and therefore the CO formation), the other challenging step along the CO-path is the oxidation of CO to form $C(OH)O^*$, which also has a very high thermodynamic penalty. In this work, to understand the fundamental reasons behind and the distinct role of O-vacancies, particularly why the CO-related intermediates are destabilized at oxygen vacancies in NiOOH, we first selected the key surface intermediates (Fig. 1) that determine the selectivity, including CH_2O^*, CHO^*, CO^*, $CH_2(OH)O^*$, $CH(OH)O^*$, $C(OH)O^*$, and $HCOO^*$, to examine their interactions and interfacial charge transfer with the catalyst surface. It is anticipated that the thermodynamic instability results from weak adsorption of the intermediates, which is normally accompanied by reduced interfacial charge transfer.

Fig. 2 shows that the charge density redistribution between these intermediates and the surface is very pronounced *via* transforming CH_2O^* into $CH_2(OH)O^*$ as opposed to that during dehydrogenating CH_2O^* to CHO^*. In the next step, the conversion of $CH_2(OH)O^*$ to $CH(OH)O^*$ reduces the charge density redistribution, while the formation of CO^* from CHO^* does so minimally. In the following steps, both transformations
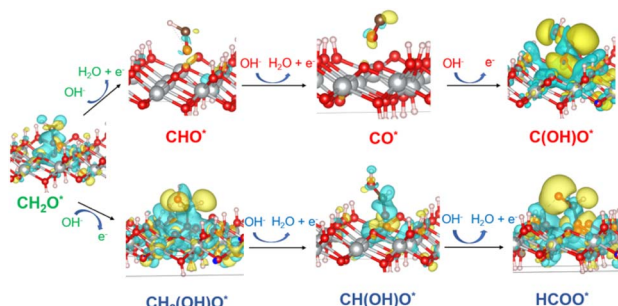

Fig. 2 Charge density differences of CH_2O^*, CHO^*, CO^*, $C(OH)O^*$, $CH_2(OH)O^*$, $CH(OH)O^*$, and $HCOO^*$ adsorbates at the O-vacant NiOOH. The charge density difference is displayed at iso-surfaces of ± 0.002 e Å^{-3}. Yellow and cyan colours are associated with electron accumulation and depletion, respectively.

from CO* to C(OH)O* and from CH(OH)O* to HCOO* result in a higher degree of the adsorbate–surface interaction.

To understand the origin of this distinct interfacial charge redistribution, we quantified the difference in the Bader charge analysis of the O of the adsorbate bonding with the O-vacant active site and that of the neighbouring Ni atoms to the vacancy, referenced to the atomic charge of corresponding atoms in the gas-phase species and the clean surface. Fig. 3 shows that the greater difference in the charge density of the relevant atoms corresponds to the more pronounced adsorbate–surface charge redistribution observed in Fig. 2. For instance, the negative charge at the O of $CH_2(OH)O^*$ and the positive charge at the neighbouring Ni accumulated significantly, showing pronounced electron transfer from the Ni to the adsorbate. In this case, the partially reduced Ni cation, because of the formation of an oxygen vacancy in its proximity, serves as an electron reservoir to stabilize the electronegative surface species. In contrast, the Bader charge difference of the O and the Ni atoms is negligible in the case of CHO*, which is in line with minimal electronic interactions between CHO* and the surface shown in Fig. 2. The consistent trend indicates that the strength of the adsorbate–surface electronic interaction is mainly attributed to the charge transfer between the O of the adsorbate and the neighbouring Ni atoms, which appears to determine the thermodynamic stability of the corresponding surface species.

Next, we explored the reaction that leads to this reduced interfacial charge transfer and the interaction of HCO* that drives the reaction to proceed via $CH_2(OH)O^*$ to form HCOO*.

The interfacial charge transfer and stability of the surface intermediates can be partially attributed to the C–O bond strength within the intermediates. In general, inserting an OH (e.g., $CH_2O^* \rightarrow CH_2(OH)O^*$) weakens the C–O bond, which allows the O to interact more strongly with the oxygen vacancy (and the neighbouring Ni atoms) and thus stabilize the adsorbate at the vacancy, promoting interfacial charge transfer as shown in Fig. 2. In contrast, eliminating a proton (e.g., $CH_2O^* \rightarrow CHO^*$) results in strengthened bonding between the C and the O within the adsorbate, leading to a lower degree of the adsorbate–surface interaction and minimizing charge transfer. However, such an explanation based on bond addition cannot explain the very unstable CHO* relative to CO*.[29] Both CHO* and CO* show similar charge transfer (Fig. 2 and 3), and the C–H bond formation in CHO* is expected to strengthen its adsorption as compared to CO*. In the following, we discuss the origin of this case (and a similar case of C(OH)O*). The typical Pt catalyst, on which CO formation and poisoning occur via partially hydrogenated CO adsorbates,[40] represents a well-known challenge[8] and is used below as a comparison.

Fig. 4 illustrates the binding configurations of representative surface intermediates of the MOR (see Fig. 2) on a Pt surface and an oxygen vacancy of NiOOH. On the Pt surface, the adsorbates typically bind with the active site via the C atom. Instead, on a NiOOH surface with an O-vacancy, the surface species adsorb on the active site through the O of its carbonyl group.[28,29,41] We find that this difference in the preferential binding mode determines the valence fulfilment of the C atom in the carbonyl group, which in turn affects the system stability.

In particular, the C atom of the CHO* or the C(OH)O* on a Pt surface can reach its full valence state by forming a strong σ bond with the metal surface. In contrast, over the NiOOH surface with an oxygen vacancy, the C atom of CHO* or C(OH)O* is unable to achieve its full valency as these species adsorb via the oxygen atom. Regardless of the possible configurations, the C in the carbonyl group CHO* remains unsaturated (Fig. 4,
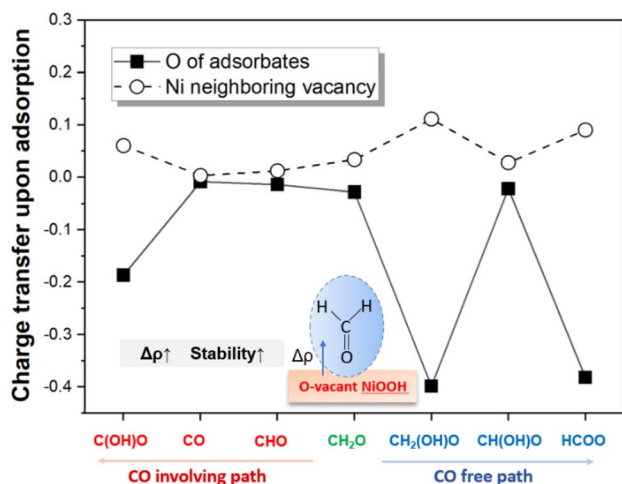

Fig. 3 Bader charge analysis of charge transfer upon adsorption of the atoms primarily involved in the electronic interaction between the adsorbate and the surface, which are referenced to the charges of corresponding atoms in the gas-phase species and on the clean surface. The relevant atoms include the O of the adsorbate bonding with the O-vacant active site (solid square symbol) and the neighbouring Ni at the oxygen vacancy (open circle symbol). Because one O-vacant active site is coordinated with three Ni atoms, the data associated with the Ni is averaged over that of the three. The positive and negative values indicate electron depletion and accumulation, respectively.
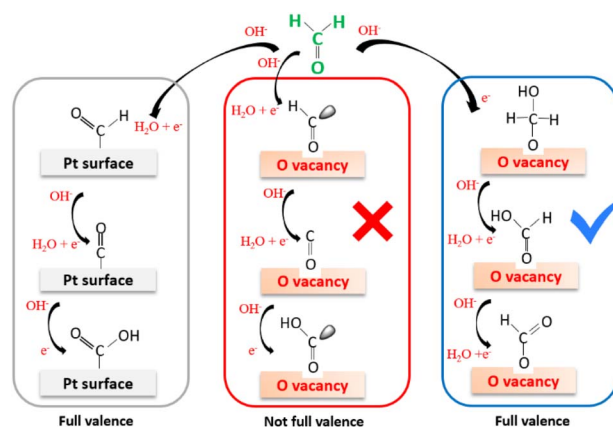

Fig. 4 Schematic illustration of the binding configurations of representative surface intermediates of the MOR (see Fig. 2) on a Pt surface and an oxygen vacancy of NiOOH. From the CH_2O intermediate, the reaction can proceed with a CO-involved pathway, which is favourable on Pt, and a CO-free pathway on defective NiOOH.

middle path) with an unpaired electron, which destabilizes the structure. This unsaturated valence of the C in CHO* is the origin of its instability, which thermodynamically impedes the transformation of CH_2O* into CHO* on the O-vacant NiOOH (the potential-limiting step for forming CO*).

The competing path to form HCOO* avoids such low-valence intermediates. To reach the full valence of carbon in the key surface intermediates over an oxygen vacancy in NiOOH, the sequence of the OH insertion and deprotonation steps should be altered; the OH insertion into CH_2O* occurs first to form $CH_2(OH)O*$ followed by deprotonation, forming $CH(OH)O*$ and HCOO* without leaving an unpaired electron in the carbon (Fig. 4 blue path). Therefore, the stability of intermediates and the reaction path is determined by the nature of the active site. Over the O-vacancies, the preferential binding configuration is different from metal catalysts to reach the full valence of the intermediates. Such preferential adsorption can also be applied to the electro-oxidation of other alcohols, such as benzyl alcohol, over Ni-based catalysts.[28] It should be noted that our current discussion is based on Ni^{3+} in NiOOH and can explain the observation of the CO-free pathway in our prior experiments.[29] The role of oxygen vacancies (and the under-coordinated Ni) in the MOR over Ni^{2+} in $Ni(OH)_2$,[13] and Ni^{4+} sites[25] at different electrode potentials could be different and remains to be explored.

Conclusions

This study provides key insights into the methanol oxidation reaction over the oxygen-vacancy active sites of NiOOH. The CO path involves a very unstable intermediate, CHO*, which shows minimum charge transfer with the oxygen vacancy and its neighbouring Ni atoms. CHO* adsorbs at the oxygen vacancy through its oxygen atom, leading to minimum interfacial charge transfer and incomplete valence saturation of the carbon in the carbonyl group. This instability effectively prevents CO formation, as confirmed by experimental results in a prior work.[29] Overall, the findings here highlight the crucial role of oxygen vacancies in promoting a CO-free MOR pathway by affecting the adsorption configuration and thermodynamic stability of key surface intermediates, thus offering valuable guidance for designing more effective and CO-tolerant catalysts in direct methanol fuel cells.

Author contributions

T. Ho, Q. P. Nguyen: data curation, visualization, concept discussion, and writing – original draft; B. Wang: conceptualization, funding acquisition, supervision, and writing – review & editing.

Conflicts of interest

There are no conflicts to declare.

Data availability

The data supporting this article have been included as part of the supplementary information (SI). Supplementary information: POSCAR files of of CH_2O*, CHO*, CO*, $C(OH)O*$, $CH_2(OH)O*$, $CH(OH)O*$, and HCOO* adsorbates at the O-vacant NiOOH. See DOI: https://doi.org/10.1039/d5ra05761b.

Acknowledgements

Notes and references

1 X. Zhao, M. Yin, L. Ma, L. Liang, C. P. Liu, J. H. Liao, T. H. Lu and W. Xing, *Energy Environ. Sci.*, 2011, **4**, 2736–2753.

2 S. K. Kamarudin, W. R. W. Daud, S. L. Ho and U. A. Hasran, *J. Power Sources*, 2007, **163**, 743–754.

3 J. M. Wang, B. X. Zhang, W. Guo, L. Wang, J. Chen, H. G. Pan and W. P. Sun, *Adv. Mater.*, 2023, **35**, 2211099.

4 Y. X. Lin, B. Geng, R. Y. Zheng, W. Chen, J. H. Zhao, H. J. Liu, Z. M. Qi, Z. P. Yu, K. Xu, X. Liu, L. Yang, L. Shan and L. Song, *Nat. Commun.*, 2025, **16**, 286.

5 M. Ahmad, M. B. Hussain, M. A. Mushtaq, W. Raza, A. Mehmood, S. Afzal, F. J. Lu, Y. W. Sui, K. Zong, X. Wang and Z. W. Chen, *Adv. Mater.*, 2025, **37**, 2502966.

6 T. Liu, Q. X. Chen, Z. He, J. L. Wang, S. Z. Sheng, J. W. Liu and S. H. Yu, *J. Am. Chem. Soc.*, 2025, **147**, 5340–5349.

7 L. Hou, C. Sun, Z. Zhang, X. Liu and J. Cho, *Small*, 2025, 2505525.

8 A. Yuda, A. Ashok and A. Kumar, *Catal. Rev.*, 2022, **64**, 126–228.

9 Y. Qin, K. Yu, G. Wang, Z. Zhuang, Y. Dou, D. Wang and Z. Chen, *Angew. Chem., Int. Ed.*, 2025, **64**, e202420817.

10 B. T. Zhu, B. Dong, F. Wang, Q. F. Yang, Y. P. He, C. J. Zhang, P. Jin and L. Feng, *Nat. Commun.*, 2023, **14**, 1686.

11 W. J. Huang, H. T. Wang, J. G. Zhou, J. Wang, P. N. Duchesne, D. Muir, P. Zhang, N. Han, F. P. Zhao, M. Zeng, J. Zhong, C. H. Jin, Y. G. Li, S. T. Lee and H. J. Dai, *Nat. Commun.*, 2015, **6**, 10035.

12 H. Y. Qin, Y. K. Ye, G. L. Lin, J. Y. Zhang, W. Q. Jia, W. Xia and L. F. Jiao, *ACS Catal.*, 2024, **14**, 16234–16244.

13 H. Cheng, B. Dong, Q. Liu and F. Wang, *J. Am. Chem. Soc.*, 2023, **145**, 26858–26862.

14 E. Antolini, J. R. C. Salgado and E. R. Gonzalez, *Appl. Catal., B*, 2006, **63**, 137–149.

15 X. Li, Y. Huang, Z. Chen, S. Hu, J. Zhu, P. Tsiakaras and P. Kang Shen, *Chem. Eng. J.*, 2023, **454**, 140131.

16 T. Xia, K. Zhao, Y. Zhu, X. Bai, H. Gao, Z. Wang, Y. Gong, M. Feng, S. Li, Q. Zheng, S. Wang, R. Wang and H. Guo, *Adv. Mater.*, 2023, **35**, 2206508.

17 S. Liu, F. Dong, Z. Tang and Q. Wang, *Int. J. Hydrogen Energy*, 2021, **46**, 15431–15441.

18 Y. Hu, P. Wu, Y. Yin, H. Zhang and C. Cai, *Appl. Catal., B*, 2012, **111**, 208–217.

19 H. Xiao, W. Wang, M. Zhao, Z. Fu, M. Bai, L. Zhang, J. Zhang, E. Luo, J. Zhang and H. Wu, *Chem. Eng. J.*, 2024, **490**, 151415.

20 C. Li, X. Chen, L. Zhang, S. Yan, A. Sharma, B. Zhao, A. Kumbhar, G. Zhou and J. Fang, *Angew. Chem.*, 2021, **133**, 7753–7758.

21 B. Zhu, J. Xiong, S. Wu, K. You, B. Sun, Y. Liu, M. Chen, P. Jin and L. Feng, *Adv. Funct. Mater.*, 2024, **34**, 2407236.

22 R. Guo, C. Liu, Y. Yang, S. Wang and L. Feng, *Chem. Sci.*, 2025, **14**, 13514–13519.

23 W. Yang, X. Yang, J. Jia, C. Hou, H. Gao, Y. Mao, C. Wang, J. Lin and X. Luo, *Appl. Catal., B*, 2019, **244**, 1096–1102.

24 X. Wang, S. Xi, W. S. V. Lee, P. Huang, P. Cui, L. Zhao, W. Hao, X. Zhao, Z. Wang and H. Wu, *Nat. Commun.*, 2020, **11**, 4647.

25 M. T. Bender, Y. C. Lam, S. Hammes-Schiffer and K. S. Choi, *J. Am. Chem. Soc.*, 2020, **142**, 21538–21547.

26 M. Y. Li, H. M. Li, K. Xiang, J. Zou, X. Z. Fu, J. L. Luo, G. Q. Luo and J. J. Zhang, *Electrochem. Energy Rev.*, 2025, **8**, 4.

27 C. Zhang, Z. Fang, H. Cheng, C. D. Jadhav, J. Nie, D. Liu, Y. Wang and Y. Liang, *J. Alloys Compd.*, 2025, **1025**, 180184.

28 L. Wei, M. D. Hossain, M. J. Boyd, J. Aviles-Acosta, M. E. Kreider, A. C. Nielander, M. B. Stevens, T. F. Jaramillo, M. Bajdich and C. Hahn, *ACS Catal.*, 2023, **13**, 4272–4282.

29 V. T. T. Phan, Q. P. Nguyen, B. Wang and I. J. Burgess, *J. Am. Chem. Soc.*, 2024, **146**, 4830–4841.

30 G. Kresse and J. Furthmüller, *Comput. Mater. Sci.*, 1996, **6**, 15–50.

31 V. T. T. Phan, Q. P. Nguyen, B. Wang and I. J. Burgess, *J. Am. Chem. Soc.*, 2025, **147**, 10758–10771.

32 M. Cococcioni and S. De Gironcoli, *Phys. Rev. B: Condens. Matter Mater. Phys.*, 2005, **71**, 035105.

33 Z. K. Goldsmith, A. K. Harshan, J. B. Gerken, M. Vörös, G. Galli, S. S. Stahl and S. Hammes-Schiffer, *Proc. Natl. Acad. Sci. U. S. A.*, 2017, **114**, 3050–3055.

34 P. E. Blochl, *Phys. Rev. B: Condens. Matter Mater. Phys.*, 1994, **50**, 17953–17979.

35 J. P. Perdew, K. Burke and M. Ernzerhof, *Phys. Rev. Lett.*, 1996, **77**, 3865–3868.

36 S. Grimme, J. Antony, S. Ehrlich and H. Krieg, *J. Chem. Phys.*, 2010, **132**, 154104.

37 J. M. P. Martirez and E. A. Carter, *Chem. Mater.*, 2018, **30**, 5205–5219.

38 R. F. W. Bader, *Chem. Rev.*, 1991, **91**, 893–928.

39 W. Tang, E. Sanville and G. Henkelman, *J. Phys.: Condens. Matter*, 2009, **21**, 084204.

40 Y. Katayama, R. Kubota, R. R. Rao, J. Hwang, L. Giordano, A. Morinaga, T. Okanishi, H. Muroyama, T. Matsui, Y. Shao-Horn and K. Eguchi, *J. Phys. Chem. C*, 2021, **125**, 26321–26331.

41 L. A. Gomez, R. Bababrik, M. R. Komarneni, J. Marlowe, T. Salavati-fard, A. D. D'Amico, B. Wang, P. Christopher and S. P. Crossley, *ACS Catal.*, 2022, **12**, 6313–6324.